Tomographic imaging of molecular orbitals

J. Itatani[1,2]**, J. Levesque**[1,3]**, D. Zeidler**[1]**, Hiromichi Niikura**[1,4]**, H. Pépin**[3]**, J. C. Kieffer**[3]**, P. B. Corkum**[1]** & D. M. Villeneuve**[1]

[1]*National Research Council of Canada, 100 Sussex Drive, Ottawa, Ontario K1A 0R6, Canada*
[2]*University of Ottawa, 150 Louis Pasteur, Ottawa, Ontario K1N 6N5, Canada*
[3]*INRS- Energie et Materiaux, 1650 boulevard Lionel-Boulet, CP 1020, Varennes, Québec J3X 1S2, Canada*
[4]*PRESTO, Japan Science and Technology Agency, 4-1-8 Honcho Kawaguchi Saitama, 332-0012, Japan*

....

Single-electron wavefunctions, or orbitals, are the mathematical constructs used to describe the multi-electron wavefunction of molecules. Because the highest-lying orbitals are responsible for chemical properties, they are of particular interest. To observe these orbitals change as bonds are formed and broken is to observe the essence of chemistry. Yet single orbitals are difficult to observe experimentally, and until now, this has been impossible on the timescale of chemical reactions. Here we demonstrate that the full three-dimensional structure of a single orbital can be imaged by a seemingly unlikely technique, using high harmonics generated from intense femtosecond laser pulses focused on aligned molecules. Applying this approach to a series of molecular alignments, we accomplish a tomographic reconstruction of the highest occupied molecular orbital of N_2. The method also allows us to follow the attosecond dynamics of an electron wave packet.

The electrons that make up molecules are organized by energy in orbitals[1,2]. Although total electron density in molecules is routinely measured by X-ray diffraction or electron scattering, only two methods are able to 'see' the highest occupied molecular orbitals (HOMOs)—electron momentum spectroscopy and scanning tunnelling microscopy. Electron momentum spectroscopy[3] is an (e, $2e$) scattering technique that can determine the radially averaged density of the outermost valence electrons. Scanning tunnelling microscopy[4] gives the electron density, distorted by surface states. We show that high harmonic emission from molecules[5–11] allows the three-dimensional shape of the highest electronic orbital to be measured, including the relative phase of components of the wavefunction. Our results may be compared with predictions of the various models that are used to describe many-electron systems[12], such as the Hartree–Fock, the Kohn–Sham and the Dyson approaches.

If we can measure orbitals with femtosecond laser technology, we can also observe orbital changes occurring on the timescale of chemical reactions. The next challenge will be to measure attosecond bound-state electron dynamics. We show that imaging orbitals can be extended to imaging coherent electron motion in atoms or molecules. Quantum mechanically, electron motion is described by a coherent superposition of electronic states. This is the closest that quantum mechanics allows to imaging the 'Bohr orbital motion' of electrons.

Tomographic imaging of a molecular orbital is achieved in three crucial steps. (1) Alignment of the molecular axis in the laboratory frame. (2) Selective ionization of the orbital. (3) Projection of the state onto a coherent set of plane waves.

Alignment of gas-phase molecules

Computed tomography refers to the technology of retrieving sectional images of an object, such as a human body, from a series of one-dimensional projections[13]. For a projection direction fixed in the laboratory frame, the object must be rotated. Thus, we begin by discussing how molecules can be aligned[14].

A relatively intense, non-resonant laser pulse induces a Stark shift of the ground state of molecules that depends on the angle of the molecular axis to the laser polarization[15]. It has been demonstrated that gas-phase molecules can be aligned adiabatically[16], aligned in three dimensions[17] or oriented[18]. We use non-adiabatic

alignment[19,20]. It results in field-free alignment of linear molecules well after the aligning pulse has terminated. A 60-fs laser pulse produces a rotational wave packet in N_2. This wave packet periodically rephases, giving periods when the molecular axes are aligned in space. The probe pulse coincides with the first half-revival at 4.1 ps (ref. 20). The degree of angular alignment is good enough to see a difference in the harmonic spectra for a 5° rotation of the alignment direction.

High harmonic generation from molecules

High harmonics are produced by ionizing atoms or molecules. We choose to operate in the tunnel ionization regime[21] because the rate of tunnel ionization depends exponentially on the ionization potential. Hence the orbital with the lowest ionization potential (the HOMO in an unexcited molecule) is preferentially selected. This is the second requirement for tomographic imaging of a single molecular orbital.

The third requirement for tomography is that we can take a series of projected images of the molecular orbital. For this we record high harmonic emission generated from the molecule itself. High harmonics have been extensively studied from atoms, whereas harmonics from molecules have been studied with isotropic distributions[5,6] or with weak alignment[7]. It has been observed[8–11] both experimentally and numerically, that harmonic emission from aligned molecules is sensitive to both the alignment angle and to the spatial structure of the electronic wavefunction. These observations provide the basis for our analysis.

High harmonic generation is understood using the three-step quasi-static model[22]—(1) tunnel ionization by an intense low-frequency laser field, (2) acceleration of the free electron, and (3) re-collision. Tunnel ionization coherently transfers a part of the bound-state electron wavefunction to the continuum. Once free, the strong laser field dominates the motion of the continuum electron wave packet. First it propagates away from the molecule (Fig. 1a) and is then driven back after the field reverses its direction. Figure 1b shows the re-colliding wave packet expanding laterally. By the time of re-collision, the electron wave packet has a typical transverse $1/e$ width of 9 Å for 800-nm laser fields[23,24]. Because the wave packet is much larger than the size of small molecules (typically ~1 Å, shown by the lines in Fig. 1b), the molecule sees essentially a plane electron wave re-colliding. We will see that the planar nature of the re-collision electron allows us to experimentally retrieve a

one-dimensional projection of the ground-state wavefunction.

The laser field shears the initial continuum wave packet in such a way that the low kinetic energy (long de Broglie wavelength) part of the wave packet re-collides first. Over the next half laser period, it chirps to high kinetic energy (short wavelength) and then back to low energy[25]. In our experiment, the highest-energy electron has a wavelength of ~1.5 Å. This wavelength is related to the high harmonic cut-off. The broad range of electron wavelengths allows us to experimentally retrieve the spatial shape of the bound-state wavefunction.

Figure 2 illustrates the final step in the harmonic generation process. Figure 2a shows a bound-state wavefunction, Ψ_g. A fraction of the electron wavefunction tunnels from this orbital. The re-colliding electron wave packet, Ψ_c, shown as a plane wave in Fig. 2b, overlaps the remaining portion of the initial wavefunction. The coherent addition of the two wavefunctions induces a dipole, seen as the asymmetric localization of electron density in Fig. 2c. The induced dipole oscillates as the continuum wavefunction propagates. It is this oscillating dipole that emits high harmonic radiation. The instantaneous frequency of the oscillating dipole is related to the electron kinetic energy by $\hbar\omega = E_k$ (refs 22, 25). In other words, the electron wave packet and the emitted photons are related by energy conservation, and are mutually coherent. We do not use the more usual expression[22], $\hbar\omega = E_k + I_p$, where I_p is the ionization potential and E_k is the instantaneous kinetic energy of the electron in the continuum at the time of re-collision calculated for a delta function potential, because here we are concerned with the electron kinetic energy seen by the bound-state electron wavefunction.

Formally, we are measuring the transition dipole moment from the highest occupied state to a set of continuum wavefunctions. Mathematically, the harmonic spectrum from a single atom or molecule is given by the Fourier transform of the dipole accelera-tion[26]. We relate the dipole acceleration spectrum to the dipole moment using the slowly varying envelope approximation (see Methods section). The spectral intensity (I) and phase of harmonics (ϕ) at frequency ω can respectively be written as $I(\omega) \propto \omega^4 |d(\omega)|^2$ and $\phi(\omega) = \arg[d(\omega)]$, where the transition dipole moment in the spectral domain is $\mathbf{d}(\omega) = a[k(\omega)] \int \psi_g(\mathbf{r})(e\mathbf{r})\exp[ik(\omega)x]\mathrm{d}\mathbf{r}$. Here the electron wave packet seen by the molecule is expanded in a superposition of plane waves as $\Psi_c = \int a(k)\exp[ik(\omega)x]\mathrm{d}k$, $k(\omega)$ is the wavenumber (momentum) of the electron corresponding to harmonic frequency ω, and $a[k(\omega)]$ is its complex amplitude[25]. A similar approach was taken by Sanpera et al.[27], who divided the electron wavefunction into bound and continuum parts and modelled the continuum part as a gaussian wave packet. Provided that $a[k(\omega)]$ is known, then measuring the harmonic spectrum—its amplitude, phase and polarization—is equivalent to measuring this integral, evaluated for different $k(\omega)$. This is an experimental determination of the one-dimensional spatial Fourier transform of $\mathbf{r}\psi_g(\mathbf{r})$.

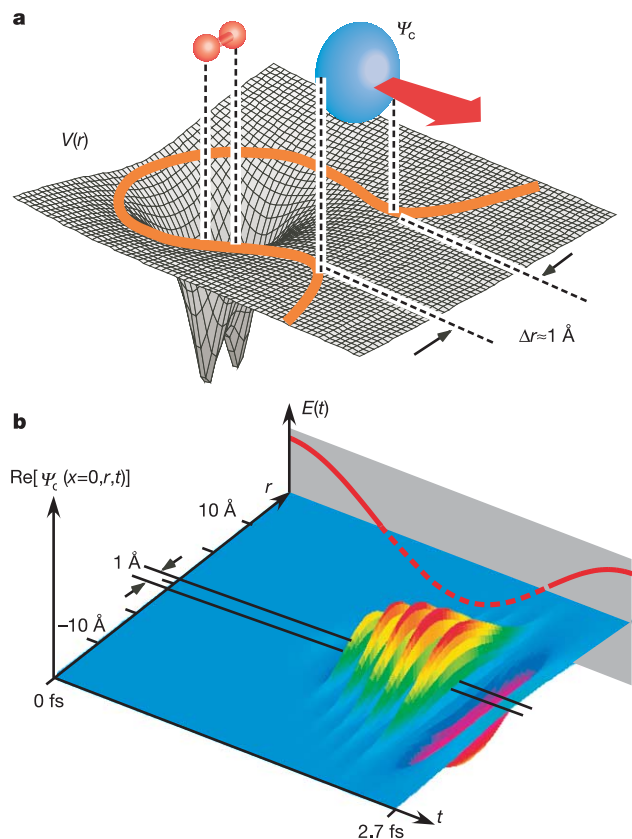Experimentally, we concentrate on a specific molecule, N_2. High

Figure 1 Illustration of the tunnel ionization process from an aligned molecule. **a**, The orange line on the potential surface is an isopotential contour slightly above the energy level of the bound state at the peak of the field amplitude. The opening of the contour shows the saddle point region where the bound-state electron wavefunction will tunnel through to the continuum. The lateral spread of the electron wave packet ψ_c is determined by the width of the saddle point region Δr that depends on the molecular alignment. The wave packet expands in the lateral direction during propagation in the continuum because of the initial momentum spread Δp given by the uncertainty principle, $\Delta p \approx h/\Delta r$. **b**, Illustration of the re-colliding wave packet seen by a molecule (the real part of the wave packet $\mathrm{Re}[\psi_c(x=0, t)]$ is shown). The kinetic energy at the time of re-collision is taken from the classical trajectory, and determines the instantaneous frequency of the wave packet as seen by the molecule. The lateral spread is calculated by the free expansion of a gaussian wave packet with an initial $1/e$ full width of 1 Å.
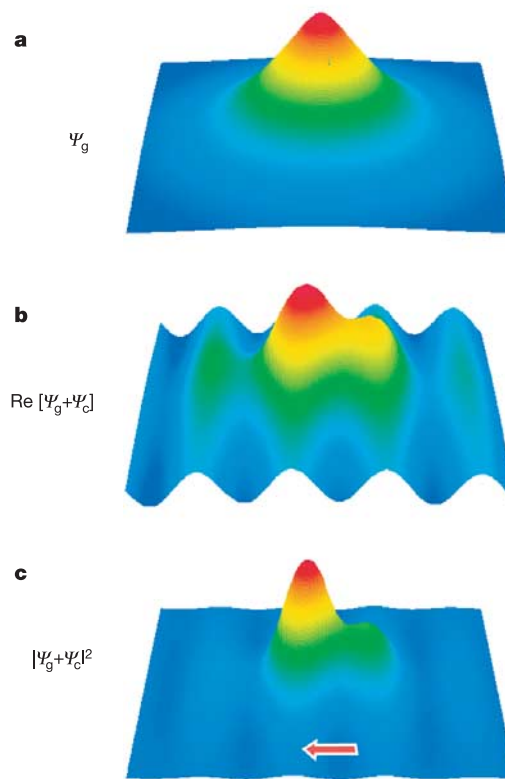

Figure 2 Illustration of a dipole induced by the superposition of a ground-state wavefunction ψ_g and a re-colliding plane wave packet ψ_c. **a**, Bound-state wavefunction (for example, H atom, 1 s). **b**, The real part of the superposition of the bound-state wavefunction ψ_g and the continuum plane wave ψ_c. **c**, The total electron density distribution $|\psi_g + \psi_c|^2$. The superposition of the two wavefunctions induces a dipole $d(t)$ as shown by the red arrow. As the wave packet propagates, the induced dipole oscillates back and forth and leads to the emission of harmonics.

harmonics are generated with a 30-fs, $2 \times 10^{14}\,W\,cm^{-2}$, 800-nm, horizontally polarized probe pulse in a $\sim 10^{17}\,cm^{-3}$ molecular gas jet described in the Methods section. The molecular alignment axis is rotated relative to the polarization of the probe pulse.

The probe pulse intensity was kept as low as possible to avoid saturation or depletion of the ground state. The molecular beam thickness was less than 1 mm and the laser focus was before the beam—conditions that minimize phase mismatch and select only the short electron trajectories[28].

Figure 3 shows the intensities of each harmonic as the laser polarization is rotated from 0 to 90° (in steps of 5°) with respect to the molecular axis. The intensity contrast between 0 and 90° exceeds an order of magnitude for some harmonics. We use these data to reconstruct the molecular orbital of N_2. Also shown is the spectrum from the reference atom, argon, recorded under conditions identical to those for the nitrogen.

Calibrating the continuum wave packet

As discussed above, the harmonic spectrum is an experimental evaluation of the dipole, $d(\omega)$. If we could evaluate the plane-wave amplitude $a[k(\omega)]$ independently, then our measurement would determine $\int \psi_g(r)(er)\exp[ik(\omega)x]dr$—that is, the spatial Fourier components of $r\psi_g(r)$. One way to do this is to perform the same experiment with a reference atom.

Argon is very similar to N_2 in its response to strong laser fields, having nearly the same ionization potential and intensity-dependent ionization probability[6]. This is confirmed by the dependence of the instantaneous ionization rates[29] for atoms, and for different orientations of N_2 (ref. 30). That means that the first, critical, step in the three-step high harmonic generation process is the same. Because the laser field dominates wave packet motion in the direction of the laser field, the second step, which determines the chirp of the re-colliding wave packets seen by Ar or N_2, will be the same. Thus, $a[k(\omega)]$ will be the same.

The continuum wave packet will also be similar for Ar and N_2. The narrow saddle point through which the electron tunnels acts as a spatial filter that removes much of the structure of the orbital from the continuum wave packet. This can be seen in numerical simulations[31]. By measuring the ellipticity dependence of the high harmonic signal[24] produced by N_2 and argon, we confirmed that the lateral spread of the wave packets is similar. The ionization rate of N_2 is angle-dependent[30,32], but is readily measured from the ion yield, and varies only by 25% for N_2 (ref. 33). This variation is almost cancelled by the angular dependence of the wave-packet
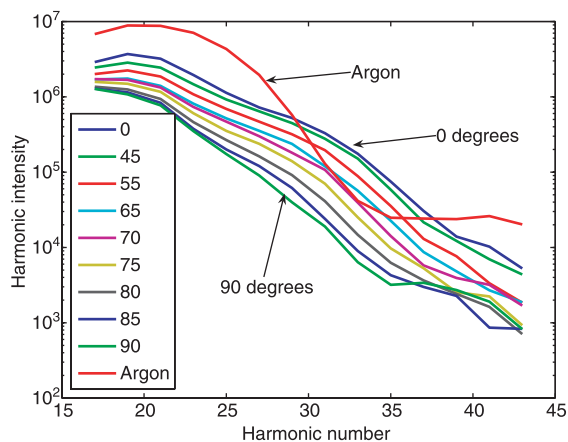
spread in the lateral direction[23]. Thus we use the harmonic spectrum from argon to determine $|a[k(\omega)]|$ without including the angular dependence of tunnel ionization rate and wave-packet spread in the continuum.

Tomographic reconstruction of the orbital

We have shown that (1) tunnel ionization, owing to its nonlinearity, is extremely selective[29,30]. In N_2, it ionizes only the highest electronic state—the HOMO. And (2), the harmonic spectra contain a range of spatial Fourier components of the shape of this single orbital. We have recorded the harmonic spectra at a series of angles between the molecular axis and the re-colliding electron. We now show that we can invert this information to obtain the shape of the orbital.

The Fourier slice theorem[13] proves that the Fourier transform of a projection P_θ is equal to a cut at angle θ through the two-dimensional Fourier transform F of the object. This is the basis of computed tomography based on the inverse Radon transform. Our dipole is the Fourier transform of a projection of the wavefunction, and so can be inverted.

We describe the mathematical details of the tomographic reconstruction in the Methods section. This procedure can reconstruct orbital shapes with symmetries such as σ_g, π_g and π_u, using harmonics 17–51 of an 800-nm laser field and 25 angles from 0° to 180° (fewer angles are needed for symmetric molecules).

A complete inversion of a general orbital requires knowledge of the relative phase and amplitude of each harmonic for two ortho-
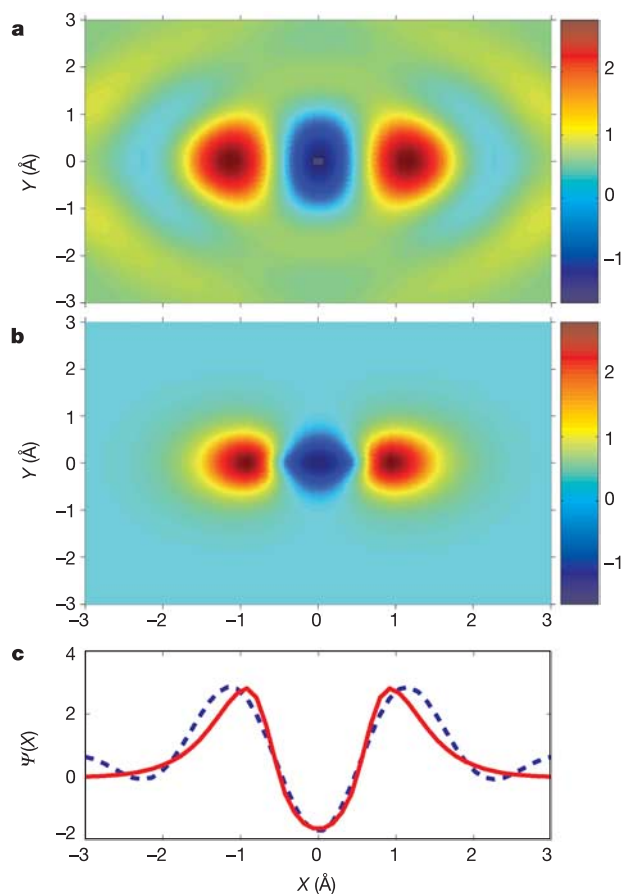

Figure 3 High harmonic spectra were recorded for N_2 molecules aligned at 19 different angles between 0 and 90° relative to the polarization axis of the laser. For clarity, only some of the angles have been plotted above. The high harmonic spectrum from argon is also shown; argon is used as the reference atom. Clearly the spectra depend on both the alignment angle and shape of the molecular orbital.

Figure 4 Molecular orbital wavefunction of N_2. **a**, Reconstructed wavefunction of the HOMO of N_2. The reconstruction is from a tomographic inversion of the high harmonic spectra taken at 19 projection angles. Both positive and negative values are present, so this is a wavefunction, not the square of the wavefunction, up to an arbitrary phase. **b**, The shape of the N_2 $2p\,\sigma_g$ orbital from an *ab initio* calculation. The colour scales are the same for both images. **c**, Cuts along the internuclear axis for the reconstructed (dashed) and *ab initio* (solid) wavefunctions.

gonal polarizations. Although we measured only the amplitude (the phase of each harmonic can be directly measured[28]) the relative phase of the harmonics is known from first principles. As with any classical or quantum resonance, a phase jump of π occurs as the driving (electron) frequency moves across resonance. Calculations by Hay *et al.*[9] show minimum harmonic signal and a π phase jump at the 25th harmonic for 0° when the re-collision electron wavelength resonates with the projected molecular dimension. We assume a phase jump of π where the measured dipole of N_2 goes through a minimum, corresponding to a change of sign of the dipole. This occurs at the 25th harmonic.

The reconstructed molecular orbital of N_2 is shown in Fig. 4a, based upon the 19 projections. It can be compared with the *ab initio* orbital calculation of the N_2 $2p$ σ_g orbital. Note that the recovered wavefunction has both positive and negative lobes, so it is not the square of the wavefunction, but the wavefunction itself, up to an arbitrary phase.

Our orbital reconstruction method is similar to medical tomography. However, we image a single orbital among many orbitals. The coherence of the re-collision provides this specificity. Of all the occupied or unoccupied states of the molecule, the re-colliding electron wave packet is only coherent with the state from which it tunnelled (or, as we will show below, with any other coherently related state). Measurable high harmonic emission requires a macroscopic number of ionizing molecules, so only the coherent emission interferes constructively and is observed experimentally. This coherent filtering is conceptually similar to the homodyne detection technique and is naturally implemented in harmonic generation.

Tomographic approaches have previously been used for molecular measurements, but in a very different way[34,35]. Although tomographic reconstruction algorithms are used, they are based on 'rotations' in the position–momentum phase-space distributions, not physical rotations of an object. These techniques yield the one-dimensional Wigner distribution $W(x,p)$ of the phase-space density of a vibrating[34] or dissociating[35] molecule. In contrast, we measure the actual three-dimensional wavefunction of a single electron orbital of a molecule.

Watching electrons move

So far, we have shown that we can take a snapshot of a molecular orbital using 30-fs laser pulses. Thus, in a pump–probe experiment, it is possible to image (probe) changes to molecular orbitals on the timescale of nuclear motion (the femtosecond timescale). However, electronic motion can be much faster. Can orbital imaging be extended to measuring electronic wave packets? We now show that the motion of this electronic wave packet can indeed be mapped to the harmonic spectrum.

It may seem that measuring wave-packet dynamics contradicts our assertion that the coherence of high harmonic generation selects a single orbital. However, an electronic wave packet is a coherent superposition of electronic states. Therefore, all states forming the wave packet are coherent with the returning electron provided it tunnelled from one or more of the states. They all contribute to the induced dipole that emits harmonics, even though only the highest-energy state contributed to the ionization. Therefore the relative intensity of each harmonic will depend on the relative phases between these electronic states.

To demonstrate how the bound-state wave-packet motion appears in harmonic spectra, we use the one-dimensional time-dependent Schrödinger equation to simulate an electron in a diatomic potential in the presence of an intense laser field. The field is chosen at a wavelength of $1.6\,\mu m$ and duration of 8 fs to induce a single re-collision. To form a fast-moving bound-state wave packet, two electronic states with energy difference of $\Delta E = 9.5\,eV$ are equally populated before the arrival of the laser pulse. This energy difference corresponds to wave-packet motion with a period of 435 as. By varying the initial phase of the two states, we perform a numerical pump–probe measurement of the wave-packet motion.

Figure 5 shows the calculated harmonic spectrum versus the initial phase of the two states. The structure in the harmonic spectrum synchronizes with the bound-state wave-packet motion. Both the modulation in the single time delay spectrum and the movement of the modulation in the pump–probe spectrum measure wave-packet dynamics.

Promises and challenges

Our experimental condition—N_2 illuminated by an 800-nm pulse at an intensity of $2 \times 10^{14}\,W\,cm^{-2}$—is not special. Ionization intensities of $\sim 10^{14}\,W\,cm^{-2}$ are typical for small- to intermediate-sized molecules[36]. For these laser parameters a re-collision electron has a wavelength of 1–2 Å—the correct range for measuring orbital structure. Thus, it appears feasible to extend tomography to many other molecules, provided there is a general method for determining $a[k(\omega)]$. This seems very promising. The phase dependence of the ionization rate determines $a[k(\omega)]$ up to a global constant describing the total ionization probability. Theories of time-dependent ionization of atoms[29] and small molecules[30] shows that the phase-dependent ionization rate is determined mainly by the ionization potential. If this remains true for more-complex molecules, then a reference atom (or molecule) can always be found to experimentally determine $a[k(\omega)]$. If a reference atom is not possible then $a[k(\omega)]$ can be characterized experimentally through the ellipticity dependence of the harmonics[24], and by directly measuring the electron spectrum in elliptically or circularly polarized light.

But does the strong electric field of the laser modify the orbital? In small molecules the modification is small, because the re-colliding electron returns near the zero-crossing of the optical field. However, it may not be small in large molecules whose bound electrons can move more freely: that is, where the molecular polarizability is larger. Thus, it may be necessary to 'shield' the orbital from the intense field. One method of shielding is to exploit traditional spectroscopy. A state, first excited by resonant light, can provide the
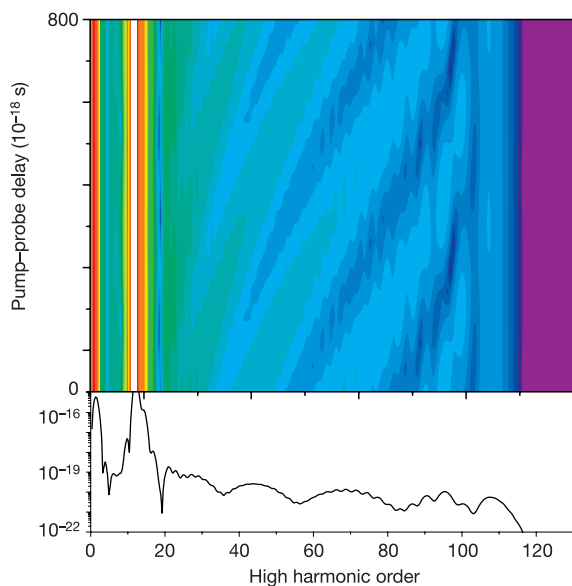
Figure 5 A one-dimensional Schrödinger calculation shows that attosecond electronic wave-packet motion is resolved in the high harmonic spectra. The bottom curve shows a spectrum at a particular pump–probe delay time; the minima are due to interference caused by the wave-packet motion. The top picture shows the spectra at a range of time delays, showing that the minima move with pump–probe time delay. The simulation populated the ground and first excited state (9.5 eV above ground) of a model atom to create an electronic wave packet.

continuum electron needed for tomography as long as it remains coherent with the ground state. Because the excited state will ionize much more easily than the ground state, tomography can be performed at field strengths in which the ground-state wavefunction is unperturbed. (Longer laser wavelengths will be required to keep the electron kinetic energy high in order to maintain sufficient spatial resolution.) Exploiting excited states has two additional advantages. First, the direction of the transition moment selects the alignment of those molecules that will ultimately ionize. Second, any orbital that is optically accessible can be imaged, not just the HOMO.

The ability of harmonics to measure the three-dimensional structure of orbitals is most important for molecular dynamics. It should be possible to observe an orbital while it changes its symmetry as a result of a curve-crossing, or to observe a chemical bond being broken—the very foundations of chemistry. With our wave-packet approach to align molecules, the only restriction is that the molecular dynamics must be faster than the duration of a rotational revival. To observe electronic rearrangement during chemical dynamics we would need to add an additional pulse to our pulse sequence[37]. Its function would be to induce dynamics. The first pulse aligns the molecule; the second one initiates the vibrational (or electronic) dynamics that we wish to study; and the final pulse would produce the harmonic radiation that could probe the evolution of the wavefunction. □

Methods

Experimental details

For all measurements, we used a pulsed gas jet with a density of $\sim 10^{17}\,\mathrm{cm}^{-3}$ in the interaction region. The laser beams were focused $\sim 1\,\mathrm{mm}$ below the orifice of the gas nozzle. The intensity of the pump pulse was set at $\sim 4 \times 10^{13}\,\mathrm{W\,cm}^{-2}$. This intensity is below the ionization threshold, where no ions are detected by a d.c.-biased electrode placed near the gas jet, and no harmonic emission is detected. The intensity of the probe pulse was estimated to be $\sim 2 \times 10^{14}\,\mathrm{W\,cm}^{-2}$ from the cut-off of high harmonics. This laser intensity is well below the saturation of ionization and harmonic generation, ensuring that high harmonics are emitted mostly at the peak of the laser pulse without depleting the ground state.

Tomographic procedure

The angular frequency ω of the radiated extreme-ultraviolet field, and the wavenumber k corresponding to the electron wave that produced it at the time of recollision, are related by $k(\omega) = (2\omega)^{1/2}$ in atomic units. The transition dipole moment between the orbital wavefunction and the continuum electron is $\mathbf{d}(\omega;\theta) = \langle\psi(\mathbf{r};\theta)|\mathbf{r}|\exp[ik(\omega)x]\rangle$. This is a complex vector, and $\psi(\mathbf{r};\theta)$ represents the orbital wavefunction rotated by Euler angle θ. Assuming perfect phase-matching, the extreme-ultraviolet signal that is emitted is given as $S(\omega;\theta) = N^2(\theta)\omega^4|a[k(\omega)]\mathbf{d}(\omega;\theta)|^2$. Here $a[k(\omega)]$ is the complex amplitude of component k of the continuum wave packet, and $N(\theta)$ is the number of ions produced.

The value of $a[k(\omega)]$ is determined experimentally by recording $S(\omega)$ for a reference argon atom whose orbital ($2p_x$), and hence $d(\omega)$, is known. Hence, $a[k(\omega)] = \omega^{-2}[S_{\mathrm{ref}}(\omega)]^{1/2}[|<\psi_{\mathrm{ref}}|r|k>|^2]^{-1/2}$. This calibration not only characterizes the continuum wave packet, it also includes experimental factors such as detector efficiency.

Then $S(\omega;\theta)$ is recorded for an unknown molecule, yielding its transition dipole moment $d(\omega;\theta)$. The definition of $d(\omega;\theta)$ is a spatial Fourier transform of the orbital in the x direction. We apply the Fourier slice theorem[13] to do the inversion, with one important modification. The Fourier transform contains the factor $\mathbf{r}$, which, being defined in the laboratory frame, does not rotate with the molecular frame, θ.

The tomographic inversion requires two intermediate functions,

$$f_x(x,y) = \sum_\theta \sum_\omega [d_x(\omega;\theta)\cos\theta + d_y(\omega;\theta)\sin\theta]\exp[ik(\omega)(x\cos\theta + y\sin\theta)]$$

$$f_y(x,y) = \sum_\theta \sum_\omega [-d_x(\omega;\theta)\sin\theta + d_y(\omega;\theta)\cos\theta]\exp[ik(\omega)(x\cos\theta + y\sin\theta)]$$

Then the wavefunction is given as:

$$\psi(x,y) = \mathrm{Re}(f_x/x + f_y/y).$$

We must also include the angle dependence of the ionization rate to normalize each spectrum. The ionization rate is known for simple molecules such as N_2 (refs 30, 32) but can be measured at the same time as the harmonic spectrum is being recorded[33] simply by measuring the total ion yield, $N(\theta)$.

1. Mulliken, R. S. Electronic structures of polyatomic molecules and valence. II. General considerations. *Phys. Rev.* **41**, 49–71 (1932).
2. Linus, C. P. *The Nature of the Chemical Bond and the Structure of Molecules and Crystals* (Cornell Univ. Press, Ithaca, New York, 1960).
3. Brion, C. E., Cooper, G., Zheng, Y., Litvinyuk, I. V. & McCarthy, I. E. Imaging of orbital electron densities by electron momentum spectroscopy—a chemical interpretation of the binary (e, 2e) reaction. *Chem. Phys.* **270**, 13–30 (2001).
4. Binning, G., Rohrer, H., Gerber, Ch. & Weibel, E. Surface studies by scanning tunneling microscopy. *Phys. Rev. Lett.* **49**, 57–61 (1982).
5. Sakai, H. & Miyazaki, K. High-order harmonic generation in nitrogen molecules with subpicosecond visible dye-laser pulses. *Appl. Phys. B* **61**, 493–498 (1995).
6. Liang, Y., Augst, A., Chin, S. L., Beaudoin, Y. & Chaker, M. High harmonic generation in atomic and diatomic molecular gases using intense picosecond laser pulses—a comparison. *J. Phys. B* **27**, 5119–5130 (1994).
7. Velotta, R., Hay, N., Manson, M. B., Castillejo, M. & Marangos, J. P. High-order harmonic generation in aligned molecules. *Phys. Rev. Lett.* **87**, 183901 (2001).
8. de Nalda, R. *et al.* Role of orbital symmetry in high-order harmonic generation from aligned molecules. *Phys. Rev. A* **69**, 031804(R) (2004).
9. Hay, N. *et al.* Investigations of electron wave-packet dynamics and high-order harmonic generation in laser-aligned molecules. *J. Mod. Opt.* **50**, 561–571 (2003).
10. Hay, N. *et al.* High-order harmonic generation in laser-aligned molecules. *Phys. Rev. A* **65**, 053805 (2002).
11. Lein, M., Corso, P. P., Marangos, J. P. & Knight, P. L. Orientation dependence of high-order harmonic generation in molecules. *Phys. Rev. A* **67**, 023819 (2003).
12. Parr, R. G. & Yang, W. *Density-functional Theory of Atoms and Molecules* (Oxford Univ. Press, New York, 1989).
13. Kak, A. C. & Slaney, M. *Principles of Computerized Tomographic Imaging* (Society for Industrial and Applied Mathematics, New York, 2001).
14. Stapelfeldt, H. & Seideman, T. Aligning molecules with strong laser pulses. *Rev. Mod. Phys.* **75**, 543–557 (2003).
15. Stapelfeldt, H., Sakai, H., Constant, E. & Corkum, P. B. Deflection of neutral molecules using the nonresonant dipole force. *Phys. Rev. Lett.* **79**, 2787–2790 (1997).
16. Sakai, H. *et al.* Controlling the alignment of neutral molecules by a strong laser field. *J. Chem. Phys.* **110**, 10235–10238 (1999).
17. Larsen, J. J., Hald, K., Bjerre, N. & Stapelfeldt, H. Three dimensional alignment of molecules using elliptically polarized laser fields. *Phys. Rev. Lett.* **85**, 2470–2473 (2000).
18. Sakai, H., Minemoto, S., Nanjo, H., Tanji, H. & Suzuki, T. Controlling the orientation of polar molecules with combined electrostatic and pulsed nonresonant laser fields. *Phys. Rev. Lett.* **90**, 083001 (2003).
19. Rosca-Pruna, F. & Vrakking, M. J. J. Experimental observation of revival structures in picosecond laser-induced alignment of I₂. *Phys. Rev. Lett.* **87**, 153902 (2001).
20. Dooley, P. W. *et al.* Direct imaging of rotational wave-packet dynamics of diatomic molecules. *Phys. Rev. A* **68**, 023406 (2003).
21. Delone, N. B. & Krainov, V. P. *Multiphoton Processes in Atoms* (Springer, Heidelberg, 2000).
22. Corkum, P. B. Plasma perspective on strong-field multiphoton ionization. *Phys. Rev. Lett.* **71**, 1994–1997 (1993).
23. Niikura, H. *et al.* Sub-laser-cycle electron pulses for probing molecular dynamics. *Nature* **417**, 917–922 (2002).
24. Dietrich, P., Burnett, N. H., Ivanov, M. & Corkum, P. B. High-harmonic generation and correlated two-electron multiphoton ionization with elliptically polarized light. *Phys. Rev. A* **50**, R3585–R3588 (1994).
25. Lewenstein, M., Balcou, Ph., Ivanov, M. Yu., L'Huillier, A. & Corkum, P. B. Theory of high-harmonic generation by low-frequency laser fields. *Phys. Rev. A* **49**, 2117–2132 (1994).
26. Burnett, K., Reed, V. C., Cooper, J. & Knight, P. L. Calculation of the background emitted during high-harmonic generation. *Phys. Rev. A* **45**, 3347–3349 (1992).
27. Sanpera, A. *et al.* Can harmonic generation cause non-sequential ionization? *J. Phys. B* **31**, L841–L848 (1998).
28. Mairesse, Y. *et al.* Attosecond synchronization of high-harmonic soft x-rays. *Science* **302**, 1540–1543 (2003).
29. Yudin, G. & Ivanov, M. Yu. Nonadiabatic tunnel ionization: Looking inside a laser cycle. *Phys. Rev. A* **64**, 013409 (2001).
30. Tong, X. M., Zhao, Z. X. & Lin, C. D. Theory of molecular tunneling ionization. *Phys. Rev. A* **66**, 033402 (2002).
31. Spanner, M., Smirnova, O., Corkum, P. B. & Ivanov, M. Yu. Reading diffraction images in strong field ionization of diatomic molecules. *J. Phys. B* **37**, L243–L250 (2004).
32. Otobe, T., Yabana, K. & Iwata, J.-I. First-principles calculations for the tunnel ionization rate of atoms and molecules. *Phys. Rev. A* **69**, 053404 (2004).
33. Litvinyuk, I. V. *et al.* Alignment-dependent strong field ionization of molecules. *Phys. Rev. Lett.* **90**, 233003 (2003).
34. Dunn, T. J., Walmsley, I. A. & Mukamel, S. Experimental determination of the quantum mechanical state of a molecular vibrational mode using fluorescence tomography. *Phys. Rev. Lett.* **74**, 884–887 (1995).
35. Skovsen, E., Stapelfeldt, H., Juhl, S. & Mølmer, K. Quantum state tomography of dissociating molecules. *Phys. Rev. Lett.* **91**, 090406 (2003).
36. Hankin, S. M., Villeneuve, D. M., Corkum, P. B., & Rayner, D. M. Nonlinear ionization of organic molecules in high intensity laser fields. *Phys. Rev. Lett.* **84**, 5082–5085 (2000).
37. Lee, K. F. *et al.* Two-pulse alignment of molecules. *J. Phys. B* **37**, L43–L48 (2004).